

DAE-Former: Dual Attention-guided Efficient Transformer for Medical Image Segmentation

Reza Azad¹

REZA.AZAD@LFB.RWTH-AACHEN.DE

René Arimond¹

RENE.ARIMOND@LFB.RWTH-AACHEN.DE

Ehsan Khodapanah Aghdam²

EHSAN.KHPAGHDAM@GMAIL.COM

Amirhossein Kazerouni³

AMIRHOSSEIN477@GMAIL.COM

Dorit Merhof^{4,5}

DORIT.MERHOF@UR.DE

¹ *Institute of Imaging and Computer Vision, RWTH Aachen University, Aachen, Germany*

² *Department of Electrical Engineering, Shahid Beheshti University, Tehran, Iran*

³ *School of Electrical Engineering, Iran University of Science and Technology, Tehran, Iran*

⁴ *Institute of Image Analysis and Computer Vision, Faculty of Informatics and Data Science, University of Regensburg, Regensburg, Germany*

⁵ *Fraunhofer Institute for Digital Medicine MEVIS, Bremen, Germany*

Abstract

Transformers have recently gained attention in the computer vision domain due to their ability to model long-range dependencies. However, the self-attention mechanism, which is the core part of the Transformer model, usually suffers from quadratic computational complexity with respect to the number of tokens. Many architectures attempt to reduce model complexity by limiting the self-attention mechanism to local regions or by redesigning the tokenization process. In this paper, we propose DAE-Former, a novel method that seeks to provide an alternative perspective by efficiently designing the self-attention mechanism. More specifically, we reformulate the self-attention mechanism to capture both spatial and channel relations across the whole feature dimension while staying computationally efficient. Furthermore, we redesign the skip connection path by including the cross-attention module to ensure the feature reusability and enhance the localization power. Our method outperforms state-of-the-art methods on multi-organ cardiac and skin lesion segmentation datasets without requiring pre-training weights. The code is publicly available at [GitHub](#).

Keywords: Transformer, Attention, Segmentation, Deep Learning, Medical.

1. Introduction

Medical image segmentation has become one of the major challenges in computer vision. For physicians to monitor diseases accurately, visualize injuries, and select the correct treatment, stable and accurate image segmentation algorithms are necessary ([Antonelli et al., 2022](#); [Kazerouni et al., 2022](#)). Deep learning networks perform very well in medical imaging, surpassing non-deep state-of-the-art (SOTA) methods. However, an immense volume of data must be trained to achieve a good generalization with a large number of network parameters ([Azad et al., 2022f](#); [Bozorgpour et al., 2021](#); [Gupta et al., 2022](#)). Additionally, the great need for large annotated data is another limitation of deep models, specifically in the medical domain. Unfortunately, per-pixel labeling is necessary for medical image

segmentation, making annotation tedious and expensive (Aghdam et al., 2022; Azad et al., 2020).

A fully convolutional neural network (FCN) is one of the pioneering works utilized for image segmentation. To preserve the spatial information and reconstruct the segmentation map, the FCN network uses convolutional layers on both encoder and decoder modules without any fully-connection, resulting in a less parametrized model and a better generalization performance. The U-Net by Ronneberger et al. (Ronneberger et al., 2015) further enhances the FCN architecture by designing skip connections in each scale of the encoder/decoder modules. Unlike FCN, U-Net performs segmentation tasks well without requiring huge annotated training sets. Skip connections can therefore be seen as the key component for the U-Net’s success (Azad et al., 2022a). Several extensions to the U-Net have been proposed to enhance the performance of the network (Zhou et al., 2018; Huang et al., 2020; Valanarasu et al., 2020). These methods aim to enrich the feature representation either by incorporating the attention mechanisms (Oktay et al., 2018; Hu et al., 2018; Woo et al., 2018), or redesigning the skip connection path (Zhou et al., 2018; Azad et al., 2019), or replacing the backbone module (Karaali et al., 2022). Although these extensions improve the feature representation, the locality restriction of the convolution layer limits the representational power of these networks to capture the shape and structural information, which is crucial for medical image segmentation. It has been shown that exploiting shape information in CNNs by fine-tuning the input images can boost the representational power of the network (Azad et al., 2021a). However, including shape representations inside the CNN networks requires modeling long-range dependencies in the latent space, which is still an open challenge in CNN architectures (Azad et al., 2021b; Feyjie et al., 2020).

To address CNN limitation, the Vision Transformer (ViT) (Dosovitskiy et al., 2020) model has been proposed. The ViT architecture is purely based on the multi-head self-attention mechanism. This enables the network to capture long-range dependencies and encode shape representations. ViT, however, requires large amounts of training data to perform similarly to CNNs, and the self-attention mechanism suffers from a quadratic computation complexity with respect to the number of tokens. The naive ViT model also renders poor performance compared to the CNN model for capturing the local representation. To address the weak local representation of the Transformer model, several methods have been proposed to build a hybrid CNN-Transformer network (Chen et al., 2021b; Heidari et al., 2022). TransUNet (Chen et al., 2021b), as a pioneer work in this direction, offers a hierarchical Transformer that captures global and fine-grained local context by combining convolutions and an attention mechanism. However, the downside of TransUNet is its high number of parameters and computational inefficiency. Additionally, although Hiformer (Heidari et al., 2022) and contextual network (Azad et al., 2022e) effectively bridge a CNN and a Transformer for medical image segmentation, it still relies on a heavy CNN backbone.

To address the computational complexity of the Transformer model, recent designs suggest either imposing a restriction on the self-attention mechanism to perform in a local region (Ding et al., 2022; Liu et al., 2021; Chen et al., 2021a), or defining a scaling factor to reduce the spatial dimension (Huang et al., 2021), or calculating channel attention instead of spatial attention (Ali et al., 2021). However, the global context is only partially captured in such methods. Swin-Unet (Cao et al., 2021) takes a different perspective and offers a U-Net-like pure Transformer architecture that operates at different scales and fuses

the features from different layers using skip connections. Swin-Unet uses two consecutive Transformer blocks with different windowing settings (shifted windows to reduce the computational burden) to attempt to recapture context from neighboring windows. Although the multi-scale representation of the Swin-Unet enhances the feature representation, the spatial context is still limited in the process.

To address the aforementioned limitations, we propose a dual attention module that operates on the full spatial dimension of the input feature, and also captures the channel context. To this end, we apply efficient attention by Shen et al. (Shen et al., 2021), which reduces the complexity of self-attention to linear while producing the same output as the regular self-attention mechanism. Moreover, to capture the input feature’s channel context, we reformulate the attention mechanism with the cross-covariance method (Ali et al., 2021). We integrate our redesigned Transformer block in a hierarchical U-Net-like pure Transformer architecture, namely, the DAE-Former. In order to reliably fuse multi-scale features from different layers, we propose a cross-attention module in each skip connection path. Our contributions are as follows: **1)** a novel efficient dual attention mechanism to capture the full spatial and channel context of the input feature vector, **2)** a skip connection cross attention (SCCA) module to adaptively fuse features from encoder and decoder layers, and **3)** a hierarchical U-Net-like pure Transformer structure for medical image segmentation.

2. Proposed Method

We introduce the DAE-Former (Figure 1), a convolution-free U-Net-like hierarchical pure Transformer. Given an input image $x^{H \times W \times C}$ with spatial dimension $H \times W$ and C channels, the DAE-Former utilizes the patch embedding module (Cao et al., 2021; Huang et al., 2021) to gain overlapping patch tokens of size 4×4 from the input image. The tokenized input ($x^{n \times d}$) then goes through the encoder module, with 3 stacked encoder blocks, each consisting of two consecutive dual Transformer layers and a patch merging layer. During patch merging, 2×2 patch tokens are merged to reduce the spatial dimension while doubling the channel dimension. This allows the network to gain a multi-scale representation in a hierarchical fashion. In the decoder, the tokens are expanded again by a factor of 2 in each block. The output of each patch expanding layer is then fused with the features forwarded by the skip connection from the parallel encoder layer using SCCA. The resulting features are fed into two consecutive dual Transformer layers. Finally, a linear projection layer produces the output segmentation map. In the next sections, we will first provide a brief overview of the efficient and transpose attentions. Then we will introduce our efficient dual attention and the SCCA modules.

2.1. Efficient Attention

The standard self-attention mechanism (1) suffers from a quadratic computational complexity ($O(N^2)$), which limits the applicability of this architecture for high-resolution images. \mathbf{Q} , \mathbf{K} , and \mathbf{V} in (1) shows the query, key, and value vectors and d is the embedding dimension,

$$S(\mathbf{Q}, \mathbf{K}, \mathbf{V}) = \text{softmax} \left(\frac{\mathbf{Q}\mathbf{K}^T}{\sqrt{d_{\mathbf{k}}}} \right) \mathbf{V}. \quad (1)$$

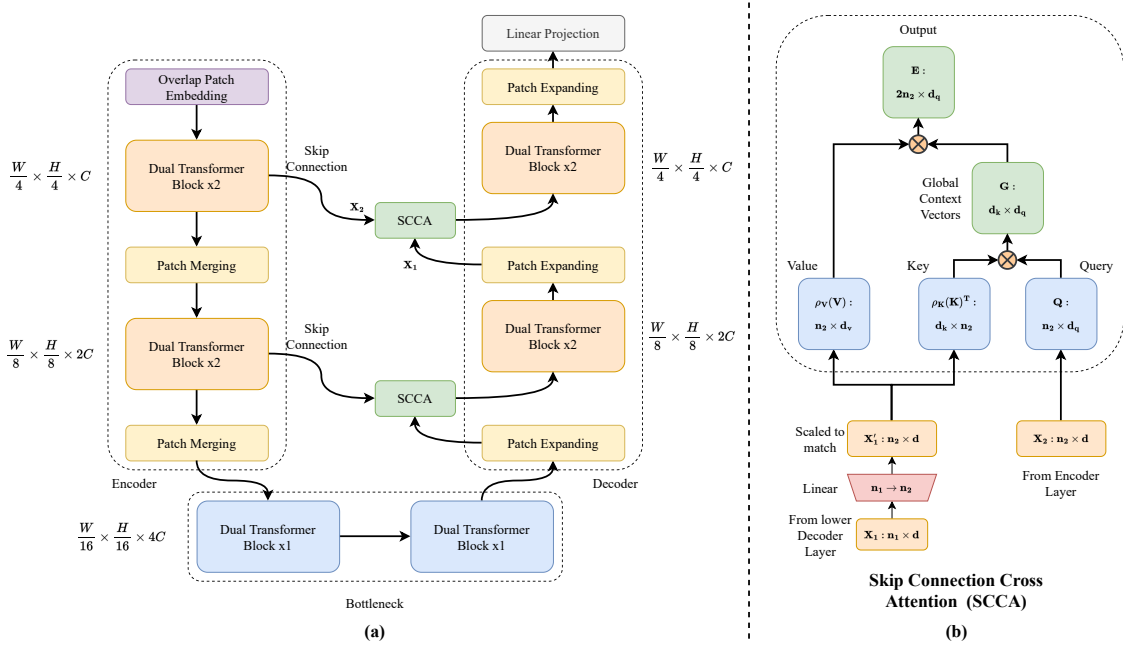


Figure 1: (a): The structure of our DAE-Former. Both the encoder and decoder of the U-Net-like architecture are each comprised of 3 blocks. Our dual attention block consists of efficient attention followed by transpose attention. (b): The skip connection cross attention (SCCA) fuses information from the encoder layers with the features from the lower decoder layer.

Efficient attention by Shen et al. (Shen et al., 2021) uses the fact that regular self-attention produces a redundant context matrix to propose an efficient way to compute the self-attention procedure (2):

$$\mathbf{E}(\mathbf{Q}, \mathbf{K}, \mathbf{V}) = \rho_q(\mathbf{Q})(\rho_k(\mathbf{K})^T \mathbf{V}), \quad (2)$$

where ρ_q and ρ_k are normalization functions for the queries and keys. It has been shown in (Shen et al., 2021) that the module produces an equivalent output of dot-product attention when ρ_q and ρ_k are applied, which are softmax normalization functions. Therefore, efficient attention normalizes the keys and queries first, then multiplies the keys and values, and finally, the resulting global context vectors are multiplied by the queries to produce the new representation.

Unlike dot-product attention, efficient attention does not first compute pairwise similarities between points. Instead, the keys are represented as d_k attention maps \mathbf{k}^T_j , with j referring to position j in the input feature. These global attention maps represent a semantic aspect of the whole input feature instead of similarities to the position of the input. This shifting of orders drastically reduces the computational complexity of the attention mechanism while maintaining high representational power. The memory complexity of efficient attention is $O(dn + d^2)$ while the computational complexity is $O(d^2n)$ when $d_v = d, d_k = \frac{d}{2}$.

which is a typical setting. In our structure, we use efficient attention to capture the spatial importance of the input feature map.

2.2. Transpose Attention

Cross-covariance attention, also called transpose attention (Ali et al., 2021), is a channel attention mechanism. This strategy employs transpose attention only to enable the processing of larger input sizes. However, we reformulate the problem and propose a transpose attention mechanism to capture the full channel dimension efficiently. The transpose attention is shown in Equation (3):

$$\mathbf{T}(\mathbf{Q}, \mathbf{K}, \mathbf{V}) = \mathbf{V}\mathcal{C}_T(\mathbf{K}, \mathbf{Q}), \quad \mathcal{C}_T(\mathbf{K}, \mathbf{Q}) = \text{Softmax}(\mathbf{K}^T\mathbf{Q}/\tau) \quad (3)$$

The keys and queries are transposed, and, therefore, the attention weights are based on the cross-covariance matrix. \mathcal{C}_T refers to the context vector of the transpose attention. The temperature parameter τ is introduced to counteract the scaling with the l_2 -norm that is applied to the queries and keys before calculating the attention weights. This increases stability during training but removes a degree of freedom, thus reducing the representational power of the module.

Transpose attention has a time complexity of $O(Nd^2/h)$, whereas standard self-attention requires $O(N^2d)$. The space complexity is $O(hN^2 + Nd)$ for transpose attention and $O(d^2/h + Nd)$ for self-attention. Self-attention scales quadratically with the number of tokens N , whereas transpose attention scales quadratically with the embedding dimension d , which is usually smaller than N , especially for larger images.

2.3. Efficient Dual Attention

A literature review (Guo et al., 2022) on the attention mechanism shows that combining spatial and channel attention enhances the capacity of the model to capture more contextual features than single attention. Therefore, we construct a dual Transformer block that combines transpose (channel) attention and efficient (spatial) attention. The structure of our efficient dual attention block is shown in Figure 2. Our efficient dual attention block (8) consists of an efficient attention (4), followed by an add & norm (5), and a transpose attention block that performs the channel attention (6), followed by an add & norm (7).

$$\mathbf{E}_{\text{block}}(\mathbf{X}, \mathbf{Q}_1, \mathbf{K}_1, \mathbf{V}_1) = \mathbf{E}(\mathbf{Q}_1, \mathbf{K}_1, \mathbf{V}_1) + \mathbf{X}, \quad (4)$$

$$\text{MLP}_1(\mathbf{E}_{\text{block}}) = \text{MLP}(\text{LN}(\mathbf{E}_{\text{block}})), \quad (5)$$

$$\mathbf{T}_{\text{block}}(\mathbf{E}_{\text{block}}, \mathbf{Q}_2, \mathbf{K}_2, \mathbf{V}_2) = \mathbf{T}(\text{MLP}_1(\mathbf{E}_{\text{block}}) + \mathbf{E}_{\text{block}}, \mathbf{Q}_2, \mathbf{K}_2, \mathbf{V}_2) + \text{MLP}_1(\mathbf{E}_{\text{block}}), \quad (6)$$

$$\text{MLP}_2(\mathbf{T}_{\text{block}}) = \text{MLP}(\text{LN}(\mathbf{T}_{\text{block}})), \quad (7)$$

$$\text{DualAttention}(\mathbf{T}_{\text{block}}) = \text{MLP}_2(\mathbf{T}_{\text{block}}) + \mathbf{T}_{\text{block}}. \quad (8)$$

$\mathbf{E}(\cdot)$, $\mathbf{T}(\cdot)$ refer to efficient attention and transpose attention, respectively. $\mathbf{T}_{\text{block}}$ denotes the transpose attention block and $\mathbf{E}_{\text{block}}$ the efficient attention block. $\mathbf{Q}_1, \mathbf{K}_1, \mathbf{V}_1$ are the keys, queries, and values calculated from the input feature \mathbf{X} . $\mathbf{Q}_2, \mathbf{K}_2, \mathbf{V}_2$ are the queries,

keys, and values computed from the input to the transpose attention block. *MLP* denotes the Mix-FFN feed-forward network (Huang et al., 2021):

$$\text{MLP}(\mathbf{X}) = \text{FC}(\text{GELU}(\text{DW-Conv}(\text{FC}(\mathbf{X})))) \quad (9)$$

with FC being a fully connected layer. GELU refers to GELU activation (Hendrycks and Gimpel, 2016) and DW-Conv is depth-wise convolution.

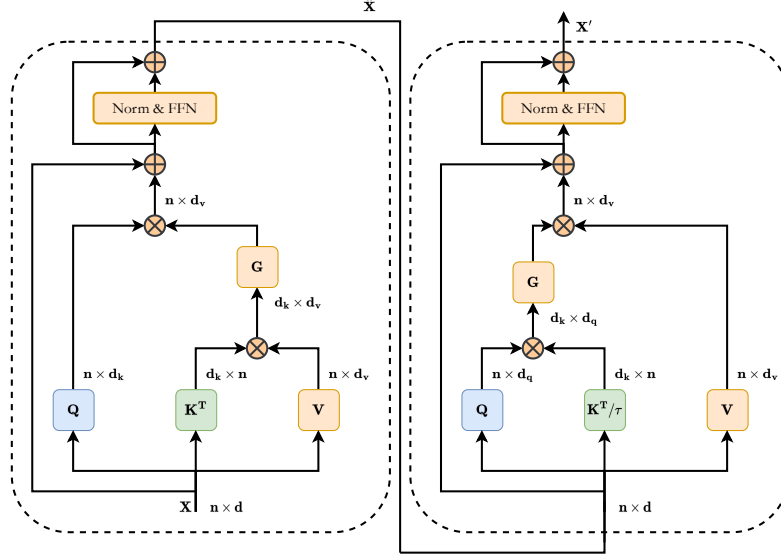


Figure 2: The efficient dual attention block. It consists of an efficient attention block, followed by a Norm & FFN, and a channel attention block followed by a Norm & FFN to perform spatial and channel attentions.

2.4. Skip Connection Cross Attention

The SCCA module is shown in Figure 1(b). Instead of simply concatenating the features from the encoder and decoder layers, we cross-attend them to preserve the underlying features more efficiently. Our proposed module can effectively provide spatial information to each decoder so that it can recover fine-grained details when producing output masks. In our structure, the skip connection cross attention (SCCA) applies efficient attention, but, instead of using the same input feature for keys, queries, and values, the input used for the query is the output of the encoder layer forwarded by a skip connection X_2 , hence the name. The input used for keys and values is the output of the lower decoder layer X_1 . To fuse the two features, X_1 needs to be scaled to the same embedding dimension as X_2 using a linear layer (10). The motivation behind using X_2 as an input for the query is to model the multi-level representation within the efficient attention block.

$$\begin{aligned} \mathbf{X}'_1 &= \text{FC}(X_1), \quad \mathbf{K}, \mathbf{V} = \text{Proj}(\mathbf{X}'_1), \quad \mathbf{Q} = \text{Proj}(X_2) \\ \mathbf{E} &= \rho_v(\mathbf{V})\rho_k(\mathbf{K}^T)\mathbf{Q}. \end{aligned} \quad (10)$$

Here, ρ_v, ρ_k are normalization functions, and $Proj$ refers to a projection function. In this case, it is a linear projection.

3. Experimental Setup

Our proposed method is implemented in an end-to-end manner using the PyTorch library and is trained on a single RTX 3090 GPU. The training is done with a batch size of 24 and a stochastic gradient descent with a base learning rate of 0.05, a momentum of 0.9, and a weight decay of 0.0001. The model is trained for 400 epochs using both cross-entropy and Dice losses ($Loss = 0.6 \cdot L_{dice} + 0.4 \cdot L_{ce}$).

3.1. Dataset and Evaluation Metrics

We use the publicly available Synapse dataset for the evaluation process, which constitutes a multi-organ segmentation dataset with 30 cases with 3779 axial abdominal clinical CT images (Cao et al., 2021; Huang et al., 2021). We follow the setting presented in (Chen et al., 2021b) for the evaluation. We further evaluate our method on the skin lesion segmentation challenge using the ISIC 2018 (Codella et al., 2019) dataset. We follow (Azad et al., 2022d) for the experimental setup.

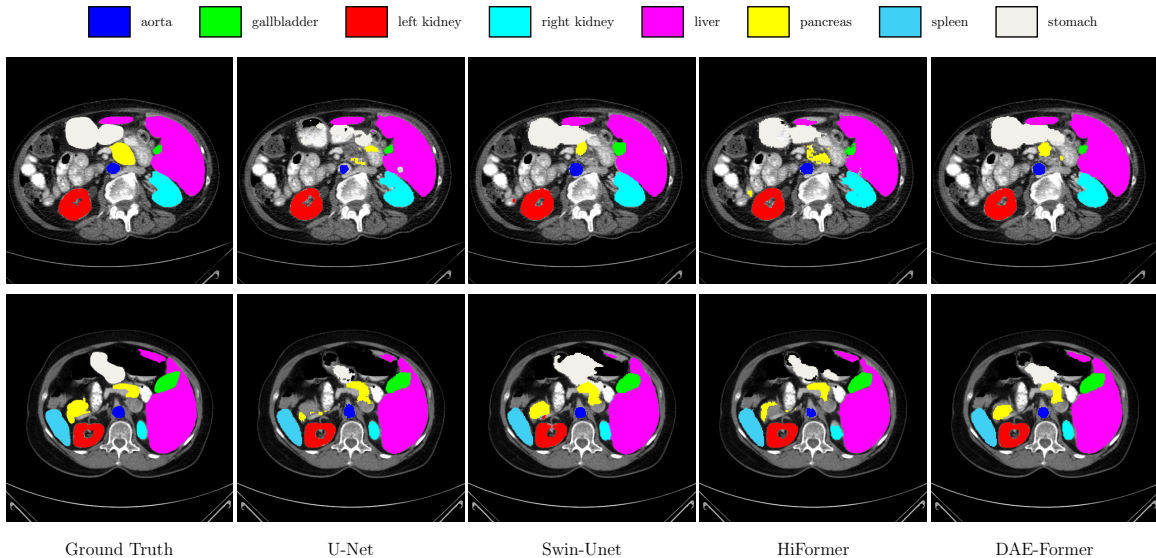
3.2. Quantitative and Qualitative Results

Table 1 presents the performance of our proposed DAE-Former on the Synapse dataset. DAE-Former surpasses the previous state-of-the-art (SOTA) methods in terms of DSC score. It also outperforms CNN-based methods by a large margin. We confirm an increase of the Dice score by 0.67% compared to the previous state-of-the-art, MISSFormer (Huang et al., 2021). We observe that the segmentation performance increases, especially for the gallbladder, kidney, liver, and spleen. Figure 3 shows the visualization of the segmentation maps. It can be observed that the competitive methods fail to predict the small organs (e.g., pancreas) while our model produces a smooth segmentation map for all organs.

The results on the skin lesion segmentation benchmarks are presented in Table 2. It can be seen that, compared to both CNN and Transformer-based methods, our network produces better performance in almost all metrics. Compared to the most competitive and

Table 1: Comparison results of the proposed method on the *Synapse* dataset. Blue indicates the best result, and red indicates the second-best. We exclusively report each method’s parameter numbers in order of millions (M).

Methods	# Params (M)	DSC \uparrow	HD \downarrow	Aorta	Gallbladder	Kidney(L)	Kidney(R)	Liver	Pancreas	Spleen	Stomach
U-Net (Ronneberger et al., 2015)	14.8	76.85	39.70	89.07	69.72	77.77	68.60	93.43	53.98	86.67	75.58
Att-UNet (Schlemper et al., 2019)	34.88	77.77	36.02	89.55	68.88	77.98	71.11	93.57	58.04	87.30	75.75
TransUNet (Chen et al., 2021b)	105.28	77.48	31.69	87.23	63.13	81.87	77.02	94.08	55.86	85.08	75.62
Swin-Unet (Cao et al., 2021)	27.17	79.13	21.55	85.47	66.53	83.28	79.61	94.29	56.58	90.66	76.60
LeVit-Unet (Xu et al., 2021)	52.17	78.53	16.84	78.53	62.23	84.61	80.25	93.11	59.07	88.86	72.76
MT-UNet (?)	79.07	78.59	26.59	87.92	64.99	81.47	77.29	93.06	59.46	87.75	76.81
TransDeepLab (Azad et al., 2022c)	21.14	80.16	21.25	86.04	69.16	84.08	79.88	93.53	61.19	89.00	78.40
HiFormer (Heidari et al., 2022)	25.51	80.39	14.70	86.21	65.69	85.23	79.77	94.61	59.52	90.99	81.08
MISSFormer (Huang et al., 2021)	42.46	81.96	18.20	86.99	68.65	85.21	82.00	94.41	65.67	91.92	80.81
EffFormer (baseline model)	22.31	80.79	17.00	85.81	66.89	84.10	81.81	94.80	62.25	91.05	79.58
DAE-Former (without SCCA)	40.75	81.59	17.31	87.41	69.57	85.22	80.46	94.68	63.71	91.47	78.23
DAE-Former	48.01	82.63	16.39	87.84	71.65	87.66	82.39	95.08	63.93	91.82	80.77

Figure 3: Comparative segmentation results on the *Synapse* dataset.

similar approach (TMU-Net), our model performs better. The TMU-Net requires extra information (boundary and foreground distribution information) and suffers from a large number of parameters (approximately 165.1M vs. 48.1M parameters for our model). We also observe that the dual attention mechanism performs better than the base structure, indicating our suggested modules' effectiveness for better performance gain. In addition, qualitative results are depicted in Appendix C.

Table 2: Performance comparison of the proposed method against the SOTA approaches on the *ISIC2018* skin lesion segmentation task.

Methods	DSC	SE	SP	ACC
U-Net (Ronneberger et al., 2015)	0.8545	0.8800	0.9697	0.9404
Att U-Net (Oktay et al., 2018)	0.8566	0.8674	0.9863	0.9376
TransUNet (Chen et al., 2021b)	0.8499	0.8578	0.9653	0.9452
MCGU-Net (Asadi-Aghbolaghi et al., 2020)	0.895	0.848	0.986	0.955
MedT (Valanarasu et al., 2021)	0.8389	0.8252	0.9637	0.9358
FAT-Net (Wu et al., 2022)	0.8903	0.9100	0.9699	0.9578
TMU-Net (Azad et al., 2022d)	0.9059	0.9038	0.9746	0.9603
Swin U-Net (Cao et al., 2021)	0.8946	0.9056	0.9798	0.9645
TransNorm (Azad et al., 2022b)	0.8951	0.8750	0.9790	0.9580
EffFormer	0.8904	0.8861	0.9698	0.9519
DAE-Former (without SCCA)	0.8962	0.8634	0.9830	0.9578
DAE-Former	0.9147	0.9120	0.9780	0.9641

To endorse the validity of the results we conducted a statistical analysis by running 10 times SOTA and our proposed models to report the mean Dice score over each organ. Figure 4 indicates that the DAE-Former performs with low variance and confident performances over Gallbladder, Kidney (L/R), and liver. We also provide attention map visualization (Figure 5) of the DAE-Former using Grad-CAM to highlight its capacity for capturing local and global dependency.

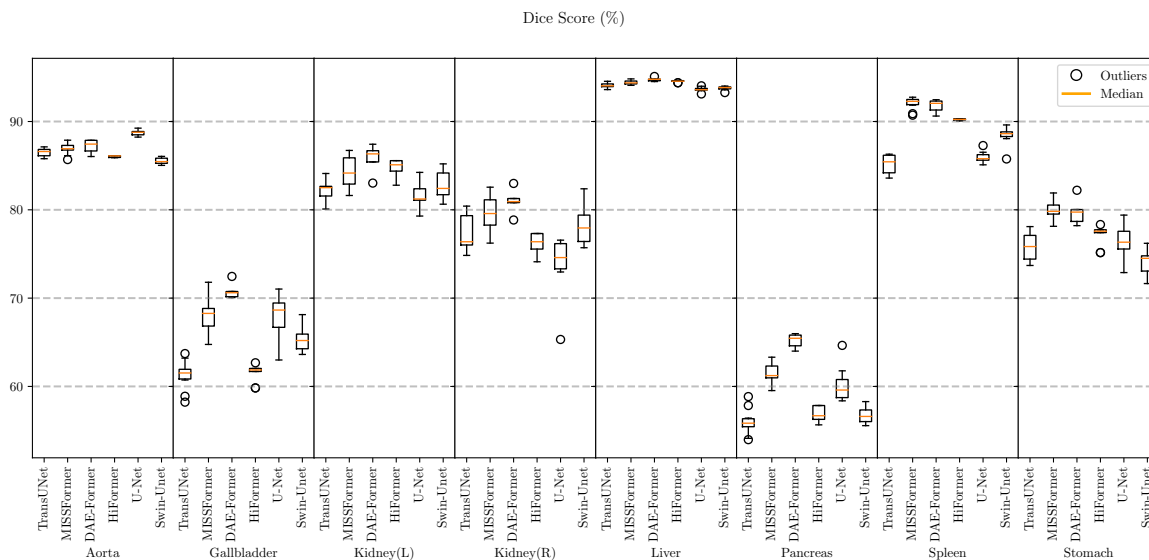


Figure 4: Statistical analysis between the U-Net (Ronneberger et al., 2015), TransUNet (Chen et al., 2021b), Swin-UNet (Cao et al., 2021), HiFormer (Heidari et al., 2022), MISSFormer (Huang et al., 2021), and our proposed method, DAE-Former.

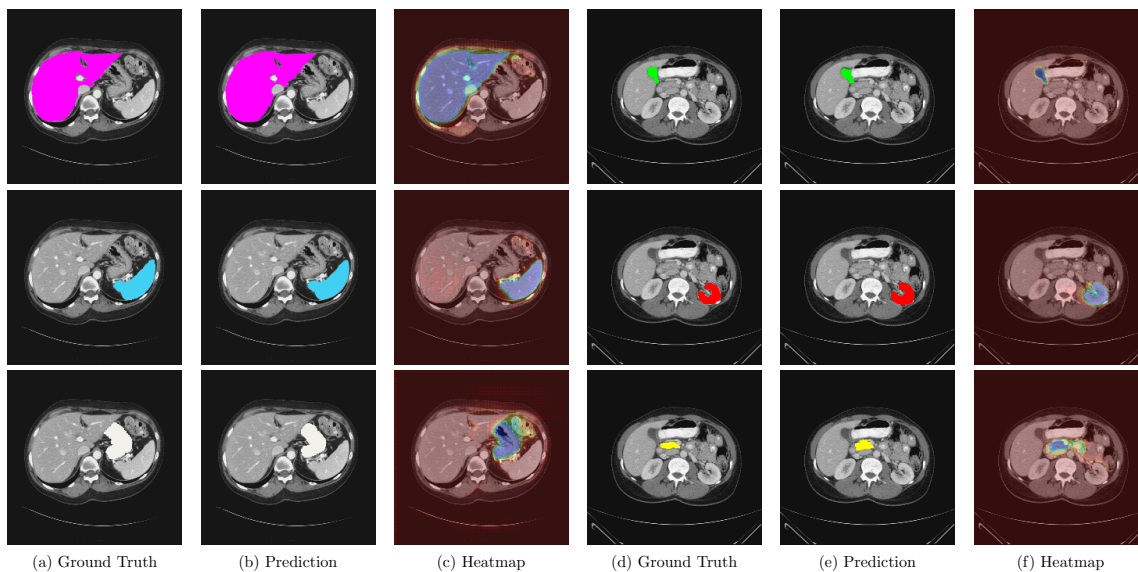


Figure 5: Visualization of attention maps using Grad-CAM on the *Synapse* dataset demonstrates the effectiveness of DAE-Former in detecting both large (liver, spleen, and stomach) and small (gallbladder, left kidney, and pancreas) organs.

4. Conclusion

In this paper, we propose DAE-Former, a novel U-Net-like hierarchical pure Transformer that leverages both spatial and channel attention on the full feature dimension. We enrich the representational space by including dual attention while retaining the same number of parameters compared to previous architectures. Furthermore, we perform a fusion of multi-scale features through skip connection cross-attention. Our model achieves the SOTA results on both the Synapse and skin lesion segmentation datasets, thereby surpassing CNN-based approaches by a large margin.

References

- Ehsan Khodapanah Aghdam, Reza Azad, Maral Zarvani, and Dorit Merhof. Attention swin u-net: Cross-contextual attention mechanism for skin lesion segmentation. *arXiv preprint arXiv:2210.16898*, 2022.
- Alaaeldin Ali, Hugo Touvron, Mathilde Caron, Piotr Bojanowski, Matthijs Douze, Armand Joulin, Ivan Laptev, Natalia Neverova, Gabriel Synnaeve, Jakob Verbeek, et al. Xcit: Cross-covariance image transformers. *Advances in neural information processing systems*, 34, 2021.
- Michela Antonelli, Annika Reinke, Spyridon Bakas, Keyvan Farahani, Annette Kopp-Schneider, Bennett A Landman, Geert Litjens, Bjoern Menze, Olaf Ronneberger, Ronald M Summers, et al. The medical segmentation decathlon. *Nature communications*, 13(1):1–13, 2022.
- Maryam Asadi-Aghbolaghi, Reza Azad, Mahmood Fathy, and Sergio Escalera. Multi-level context gating of embedded collective knowledge for medical image segmentation. *arXiv preprint arXiv:2003.05056*, 2020.
- Reza Azad, Maryam Asadi-Aghbolaghi, Mahmood Fathy, and Sergio Escalera. Bi-directional convlstm u-net with densely connected convolutions. In *Proceedings of the IEEE/CVF international conference on computer vision workshops*, pages 0–0, 2019.
- Reza Azad, Maryam Asadi-Aghbolaghi, Mahmood Fathy, and Sergio Escalera. Attention deeplabv3+: Multi-level context attention mechanism for skin lesion segmentation. In *European Conference on Computer Vision*, pages 251–266. Springer, 2020.
- Reza Azad, Afshin Bozorgpour, Maryam Asadi-Aghbolaghi, Dorit Merhof, and Sergio Escalera. Deep frequency re-calibration u-net for medical image segmentation. In *Proceedings of the IEEE/CVF International Conference on Computer Vision*, pages 3274–3283, 2021a.
- Reza Azad, Abdur R Fayjie, Claude Kauffmann, Ismail Ben Ayed, Marco Pedersoli, and Jose Dolz. On the texture bias for few-shot cnn segmentation. In *Proceedings of the IEEE/CVF Winter Conference on Applications of Computer Vision*, pages 2674–2683, 2021b.

- Reza Azad, Ehsan Khodapanah Aghdam, Amelie Rauland, Yiwei Jia, Atlas Haddadi Avval, Afshin Bozorgpour, Sanaz Karimijafarbigloo, Joseph Paul Cohen, Ehsan Adeli, and Dorit Merhof. Medical image segmentation review: The success of u-net. *arXiv preprint arXiv:2211.14830*, 2022a.
- Reza Azad, Mohammad T Al-Antary, Moein Heidari, and Dorit Merhof. Transnorm: Transformer provides a strong spatial normalization mechanism for a deep segmentation model. *IEEE Access*, 10:108205–108215, 2022b.
- Reza Azad, Moein Heidari, Moein Shariatnia, Ehsan Khodapanah Aghdam, Sanaz Karimijafarbigloo, Ehsan Adeli, and Dorit Merhof. Transdeeplab: Convolution-free transformer-based deeplab v3+ for medical image segmentation. In *Predictive Intelligence in Medicine*, pages 91–102. Springer Nature Switzerland, 2022c.
- Reza Azad, Moein Heidari, Yuli Wu, and Dorit Merhof. Contextual attention network: Transformer meets u-net. In *International Workshop on Machine Learning in Medical Imaging*, pages 377–386. Springer, 2022d.
- Reza Azad, Moein Heidari, Yuli Wu, and Dorit Merhof. Contextual attention network: Transformer meets u-net. *arXiv preprint arXiv:2203.01932*, 2022e.
- Reza Azad, Nika Khosravi, Mohammad Dehghanmanshadi, Julien Cohen-Adad, and Dorit Merhof. Medical image segmentation on mri images with missing modalities: A review. *arXiv preprint arXiv:2203.06217*, 2022f.
- Afshin Bozorgpour, Reza Azad, Eman Showkatian, and Alaa Sulaiman. Multi-scale regional attention deeplab3+: Multiple myeloma plasma cells segmentation in microscopic images. In *Proceedings of the MICCAI Workshop on Computational Pathology*, volume 156 of *Proceedings of Machine Learning Research*, pages 47–56. PMLR, 2021.
- Hu Cao, Yueyue Wang, Joy Chen, Dongsheng Jiang, Xiaopeng Zhang, Qi Tian, and Manning Wang. Swin-unet: Unet-like pure transformer for medical image segmentation. *arXiv preprint arXiv:2105.05537*, 2021.
- Chun-Fu Chen, Rameswar Panda, and Quanfu Fan. Regionvit: Regional-to-local attention for vision transformers. *arXiv preprint arXiv:2106.02689*, 2021a.
- Jieneng Chen, Yongyi Lu, Qihang Yu, Xiangde Luo, Ehsan Adeli, Yan Wang, Le Lu, Alan L Yuille, and Yuyin Zhou. Transunet: Transformers make strong encoders for medical image segmentation. *arXiv preprint arXiv:2102.04306*, 2021b.
- Liang-Chieh Chen, Yukun Zhu, George Papandreou, Florian Schroff, and Hartwig Adam. Encoder-decoder with atrous separable convolution for semantic image segmentation. In *Proceedings of the European conference on computer vision (ECCV)*, pages 801–818, 2018.
- Noel Codella, Veronica Rotemberg, Philipp Tschandl, M Emre Celebi, Stephen Dusza, David Gutman, Brian Helba, Aadi Kalloo, Konstantinos Liopyris, Michael Marchetti, et al. Skin lesion analysis toward melanoma detection 2018: A challenge hosted by the international skin imaging collaboration (isic). *arXiv preprint arXiv:1902.03368*, 2019.

- Mingyu Ding, Bin Xiao, Noel Codella, Ping Luo, Jingdong Wang, and Lu Yuan. Davit: Dual attention vision transformers. *arXiv preprint arXiv:2204.03645*, 2022.
- Alexey Dosovitskiy, Lucas Beyer, Alexander Kolesnikov, Dirk Weissenborn, Xiaohua Zhai, Thomas Unterthiner, Mostafa Dehghani, Matthias Minderer, Georg Heigold, Sylvain Gelly, et al. An image is worth 16x16 words: Transformers for image recognition at scale. *arXiv preprint arXiv:2010.11929*, 2020.
- Abdur R Feyjie, Reza Azad, Marco Pedersoli, Claude Kauffman, Ismail Ben Ayed, and Jose Dolz. Semi-supervised few-shot learning for medical image segmentation. *arXiv preprint arXiv:2003.08462*, 2020.
- Meng-Hao Guo, Tian-Xing Xu, Jiang-Jiang Liu, Zheng-Ning Liu, Peng-Tao Jiang, Tai-Jiang Mu, Song-Hai Zhang, Ralph R Martin, Ming-Ming Cheng, and Shi-Min Hu. Attention mechanisms in computer vision: A survey. *Computational Visual Media*, pages 1–38, 2022.
- Anubha Gupta, Shiv Gehlot, Shubham Goswami, Sachin Motwani, Ritu Gupta, Álvaro García Faura, Dejan Štepec, Tomaž Martinčič, Reza Azad, Dorit Merhof, et al. Segpc-2021: A challenge & dataset on segmentation of multiple myeloma plasma cells from microscopic images. *Medical Image Analysis*, page 102677, 2022.
- Moein Heidari, Amirhossein Kazerooni, Milad Soltany, Reza Azad, Ehsan Khodapanah Aghdam, Julien Cohen-Adad, and Dorit Merhof. Hiformer: Hierarchical multi-scale representations using transformers for medical image segmentation. *arXiv preprint arXiv:2207.08518*, 2022.
- Dan Hendrycks and Kevin Gimpel. Gaussian error linear units (gelus). *arXiv preprint arXiv:1606.08415*, 2016.
- Jie Hu, Li Shen, and Gang Sun. Squeeze-and-excitation networks. In *Proceedings of the IEEE conference on computer vision and pattern recognition*, pages 7132–7141, 2018.
- Huimin Huang, Lanfen Lin, Ruofeng Tong, Hongjie Hu, Qiaowei Zhang, Yutaro Iwamoto, Xianhua Han, Yen-Wei Chen, and Jian Wu. Unet 3+: A full-scale connected unet for medical image segmentation. In *ICASSP 2020-2020 IEEE International Conference on Acoustics, Speech and Signal Processing (ICASSP)*, pages 1055–1059. IEEE, 2020.
- Xiaohong Huang, Zhifang Deng, Dandan Li, and Xueguang Yuan. Missformer: An effective medical image segmentation transformer. *arXiv preprint arXiv:2109.07162*, 2021.
- Ali Karaali, Rozenn Dahyot, and Donal J Sexton. Dr-vnet: Retinal vessel segmentation via dense residual unet. In *International Conference on Pattern Recognition and Artificial Intelligence*, pages 198–210. Springer, 2022.
- Amirhossein Kazerooni, Ehsan Khodapanah Aghdam, Moein Heidari, Reza Azad, Mohsen Fayyaz, Ilker Hacihaliloglu, and Dorit Merhof. Diffusion models for medical image analysis: A comprehensive survey. *arXiv preprint arXiv:2211.07804*, 2022.

- Ze Liu, Yutong Lin, Yue Cao, Han Hu, Yixuan Wei, Zheng Zhang, Stephen Lin, and Baining Guo. Swin transformer: Hierarchical vision transformer using shifted windows. In *Proceedings of the IEEE/CVF International Conference on Computer Vision*, pages 10012–10022, 2021.
- Ozan Oktay, Jo Schlemper, Loic Le Folgoc, Matthew Lee, Mattias Heinrich, Kazunari Misawa, Kensaku Mori, Steven McDonagh, Nils Y Hammerla, Bernhard Kainz, et al. Attention u-net: Learning where to look for the pancreas. *arXiv preprint arXiv:1804.03999*, 2018.
- Olaf Ronneberger, Philipp Fischer, and Thomas Brox. U-net: Convolutional networks for biomedical image segmentation. In *International Conference on Medical image computing and computer-assisted intervention*, pages 234–241. Springer, 2015.
- Jo Schlemper, Ozan Oktay, Michiel Schaap, Mattias Heinrich, Bernhard Kainz, Ben Glocker, and Daniel Rueckert. Attention gated networks: Learning to leverage salient regions in medical images. *Medical image analysis*, 53:197–207, 2019.
- Zhuoran Shen, Mingyuan Zhang, Haiyu Zhao, Shuai Yi, and Hongsheng Li. Efficient attention: Attention with linear complexities. In *Proceedings of the IEEE/CVF winter conference on applications of computer vision*, pages 3531–3539, 2021.
- Jeya Maria Jose Valanarasu, Vishwanath A Sindagi, Ilker Hacihaliloglu, and Vishal M Patel. Kiu-net: Towards accurate segmentation of biomedical images using over-complete representations. In *International conference on medical image computing and computer-assisted intervention*, pages 363–373. Springer, 2020.
- Jeya Maria Jose Valanarasu, Poojan Oza, Ilker Hacihaliloglu, and Vishal M Patel. Medical transformer: Gated axial-attention for medical image segmentation. In *International Conference on Medical Image Computing and Computer-Assisted Intervention*, pages 36–46. Springer, 2021.
- Sanghyun Woo, Jongchan Park, Joon-Young Lee, and In So Kweon. Cbam: Convolutional block attention module. In *Proceedings of the European conference on computer vision (ECCV)*, pages 3–19, 2018.
- Huisi Wu, Shihuai Chen, Guilian Chen, Wei Wang, Baiying Lei, and Zhenkun Wen. Fat-net: Feature adaptive transformers for automated skin lesion segmentation. *Medical Image Analysis*, 76:102327, 2022.
- Guoping Xu, Xingrong Wu, Xuan Zhang, and Xinwei He. Levit-unet: Make faster encoders with transformer for medical image segmentation. *arXiv preprint arXiv:2107.08623*, 2021.
- Zongwei Zhou, Md Mahfuzur Rahman Siddiquee, Nima Tajbakhsh, and Jianming Liang. Unet++: A nested u-net architecture for medical image segmentation. In *Deep learning in medical image analysis and multimodal learning for clinical decision support*, pages 3–11. Springer, 2018.

Appendix A. Attention in Detail

In this section, we elaborate more on our proposed method’s attention mechanism and design choice. Initially, we visualize the standard self-attention, efficient self-attention (Shen et al., 2021) and transposed self-attention (Ali et al., 2021) modules in Figure 6. The standard self-attention performs the calculation based on the tokens and is, therefore, not an ideal choice for high-resolution images. The efficient attention module, however, first multiplies the keys and values to obtain a global context vector. The resulting calculation requires the keys and queries to be normalized beforehand to obtain the same result as self-attention, but the computational complexity is linear with respect to the number of tokens. Transpose attention (Figure 6(c)) is also linear, but due to the keys being transposed, the attention is calculated on the channel dimension of the input tensor.

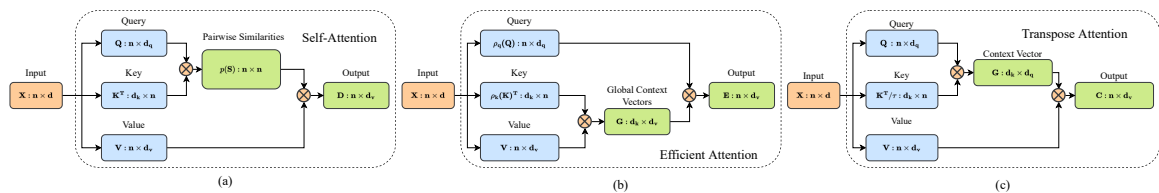


Figure 6: (a) Standard dot-product attention, (b) efficient attention (Shen et al., 2021), and (c) transpose attention (Ali et al., 2021). Redrawn for comparative overview.

In our method, we take into account the computational advantages of the efficient and the transpose attention mechanisms to build a dual attention mechanism (channel and spatial attentions as presented in the main text). There are several ways in which the channel and spatial attention blocks may be combined. The first option is to employ sequential dual attention. Here, the channel attention block is applied to the output of the efficient spatial attention block or vice versa. The two attention blocks can be computed in parallel on the same input. The outputs of both blocks must be combined, which presents more options: The tensors can either be added, which is referred to as “additive dual attention,” or concatenated and fed to an MLP, which reduces the dimension to the input dimension.

Four different possibilities are explored in this ablation study. These structures are shown in Figure 7. The first is sequential dual attention, as already explained in the methods section. Next, two variants for additive dual attention were tested; namely, simple additive dual attention (Figure 7(b)) and complex additive dual attention (Figure 7(c)). The former was expected to have a more unstable backpropagation as the outputs of each attention block are not normalized. Although the latter has a larger number of parameters, the outputs of efficient and channel attention were normalized and fed to an FFN before the addition. Lastly, the concatenation dual attention is shown in Figure 7(d). The outputs of both blocks are normalized, then concatenated. An MLP reduces the dimension from twice the input dimension back to the input dimension, and the resulting tensor is again normalized.

The performance of the described dual attention modules was tested on the Synapse dataset. The network used is the same as shown in Figure 1, but the dual attention module

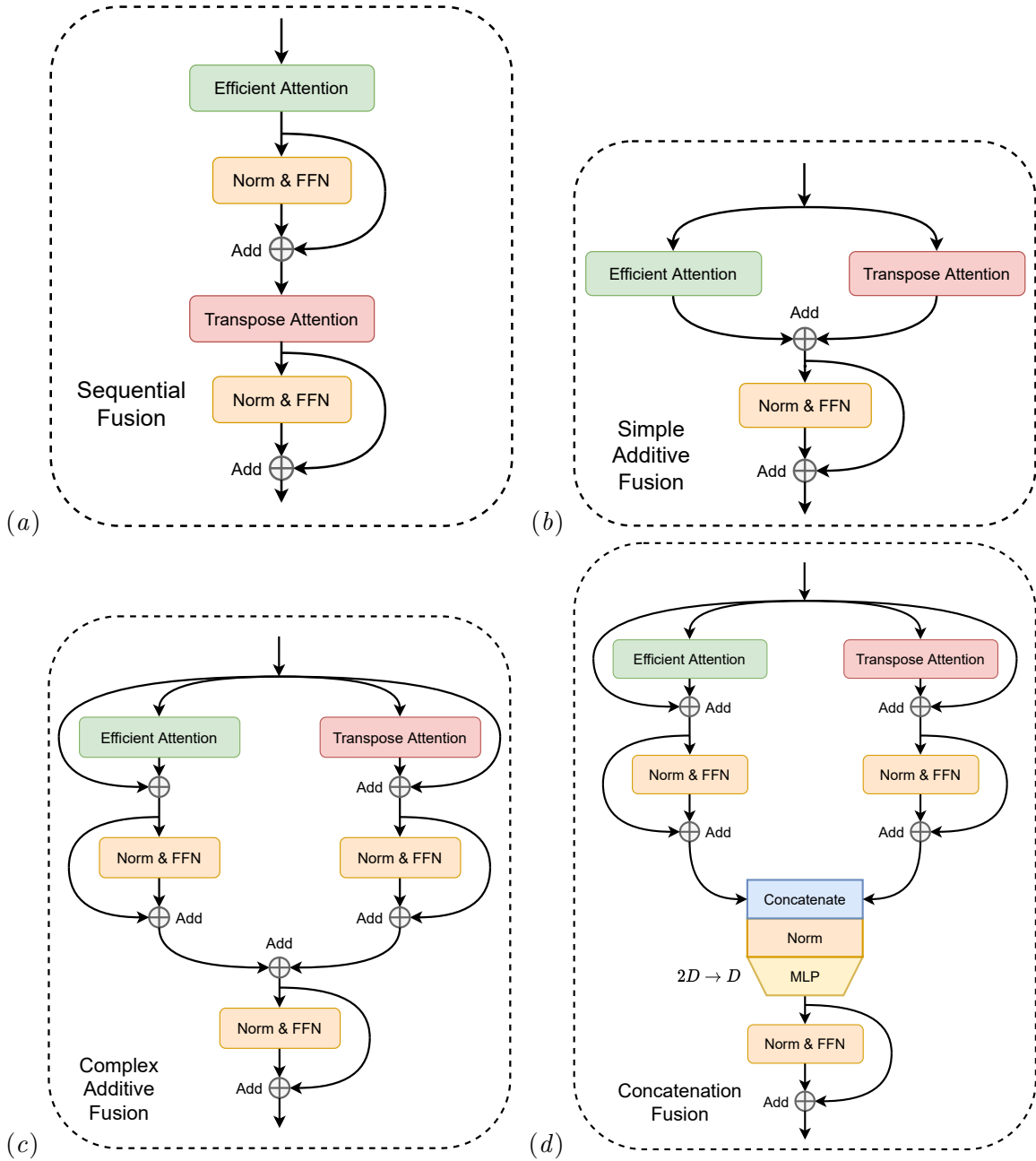


Figure 7: (a) Sequential dual attention, (b) simple additive dual attention, (c) complex additive dual attention, and (d) concatenation dual attention.

is replaced by the modified versions. The initial learning rate was set to 0.05 and the batch size to 24. A comparison is shown in Table 3. As can be seen, sequential fusion outperforms

Dual Attention Strategy	# Params [M]	DSC	HD
Sequential	48.1	82.63	17.46
Simple Additive	48.0	79.51	23.83
Complex Additive	61.1	81.49	19.36
Concatenation	64.0	80.11	27.20

Table 3: Performance comparison of dual attention variations on the Synapse dataset.

all the variants, with both the lowest required parameters and the best scores. Hence, we used it for all layers in the proposed network.

Appendix B. Input Resolution and Skip Connection Effect

We also explore the effect of skip connections in our suggested network. In this respect, we reconstructed our model with three settings: no skip connections, one skip connection in the highest layer, and two skip connections, i.e. the base setting. The results are presented in Table 4. We observe that the model behaves as expected: The more skip connections there are, the better the performance. In particular, fine-grained information from higher layers is critical to the fusion of information.

# Skip Connections	DSC	HD
0	79.71	22.46
1	81.81	21.66
2	82.63	17.46

Table 4: Performance comparison for different numbers of skip connections. Experiments are done on the Synapse dataset.

To evaluate the effect of image resolution, we conducted experiments with two different image resolutions besides the original 224×224 resolution that we use in our experiments. In this respect, we reduced the input size to 128×128 pixels to observe the low-resolution impact. Furthermore, we slightly increased the image resolution to 288×288 pixels to analyze the effect of higher resolution. The results are shown in Table 5. As expected, the performance increases for high resolution, as more fine-grained information is available.

Appendix C. Further Visualization Results

To further provide an insight into the segmentation capacity of the network, we provided comparative visualization results of the network on the skin lesion segmentation task in Figure 8. It can be observed that our method estimates the skin lesion regions with varying shapes and patterns. Moreover, compared to the SOTA approaches, our method has a better prediction of the lesion boundary.

Image Size	DSC	HD
128×128	79.20	15.90
$224 \times 224^\dagger$	82.43	17.46
288×288	82.68	17.85

Table 5: Performance comparison for different image size settings. The symbol \dagger indicates the original setting through this study.

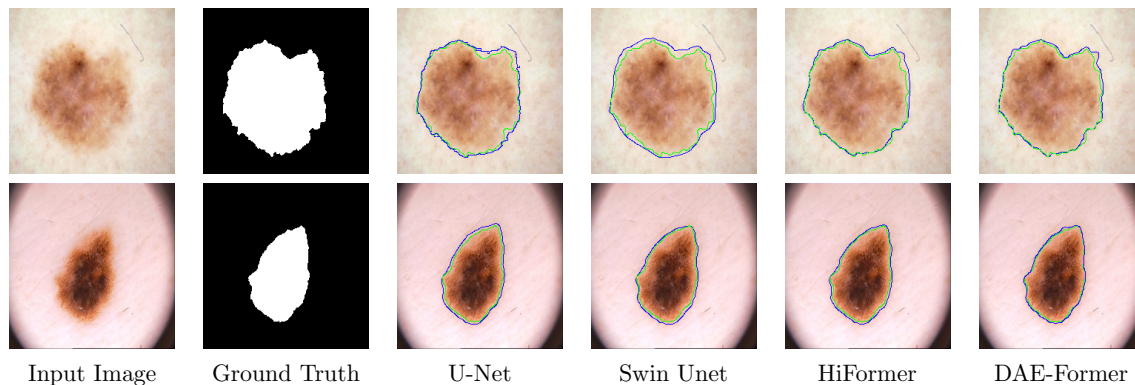


Figure 8: Visual comparisons of different methods on the *ISIC2018* skin lesion dataset. Ground truth boundaries are shown in green, and predicted boundaries are shown in blue.

Appendix D. Computational Complexity

The number of parameters used by the DAE-Former is shown in Table 6. As can be seen, although the DAE-Former has a comparable number of parameters to the MISSFormer, it has a slightly better performance.

Table 6: Comparison of the number of parameters.

Methods	# Params [M]	DSC \uparrow	HD \downarrow
DeepLapv3+ (CNN) (Chen et al., 2018)	59.50	77.63	39.95
Swin-Unet (Cao et al., 2021)	27.17	79.13	21.55
TransUNet (Chen et al., 2021b)	105.28	77.48	31.69
LeVit-Unet (Xu et al., 2021)	52.17	78.53	16.84
MISSFormer (Huang et al., 2021)	42.5	81.96	18.20
HiFormer (Heidari et al., 2022)	25.51	80.39	14.70
DAE-Former	48.1	82.63	17.46

In order to compare the trade-off between efficiency and performance, we provided Figure 9. In our visualization, we normalized each metric into the range 0-1, and then reversed the HD distance and the number of parameters to match the DSC score. It can be observed

that our network performs better compared to other models with considerably lower parameters. TransUNet (Chen et al., 2021b), for instance, requires 105.28M parameters, and its value is close to zero, whereas ours uses 48.1M parameters and achieves a significantly better Dice score and HD distance with 4.95 and 14.23 differences, respectively.

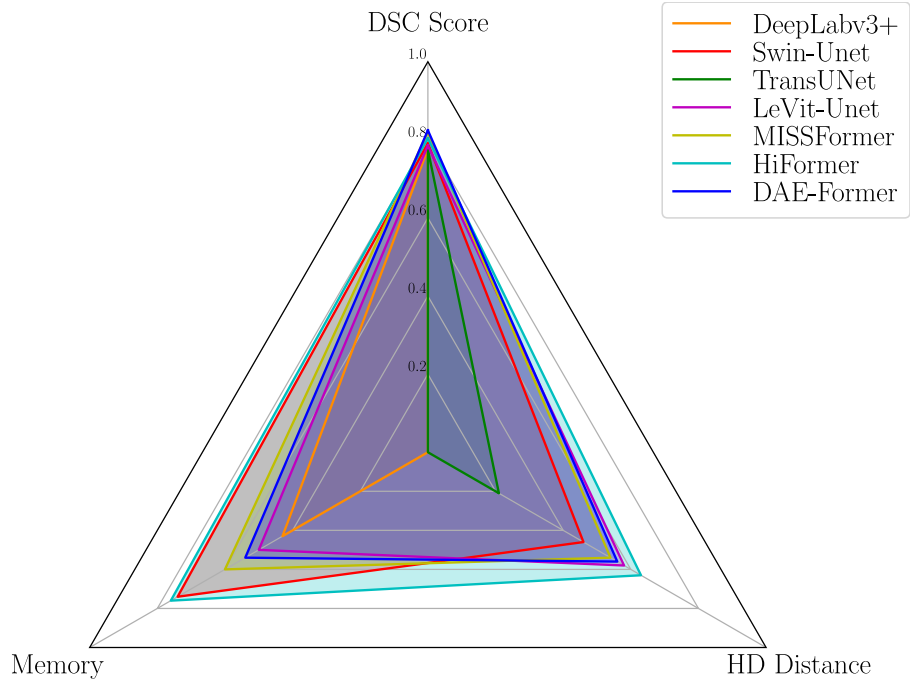


Figure 9: Efficiency vs performance chart of the SOTA approaches against our suggested network.